ACS APPLIED MATERIALS & INTERFACES

Letter

www.acsami.org

Temperature-Dependent Thermal Properties of Supported MoS_2 Monolayers

Andrzej Taube,† Jarosław Judek, Anna Łapińska, and Mariusz Zdrojek*

Faculty of Physics, Warsaw University of Technology, Koszykowa 75, 00-662 Warsaw, Poland

Supporting Information

ABSTRACT: Thermal properties can substantially affect the operation of various electronics and optoelectronics devices based on two-dimensional materials. In this work, we describe our investigation of temperature-dependent thermal conductivity and interfacial thermal conductance of molybdenum disulfide monolayers supported on SiO_2/Si substrates, using Raman spectroscopy. We observed that the calculated thermal conductivity (κ) and interfacial thermal conductance (g) decreased with increasing temperature from 62.2 W m^{-1} K^{-1} and 1.94 MW m^{-2} K^{-1} at 300 K to 7.45 W m^{-1} K^{-1} and 1.25 MW m^{-2} K^{-1} at 450 K, respectively.

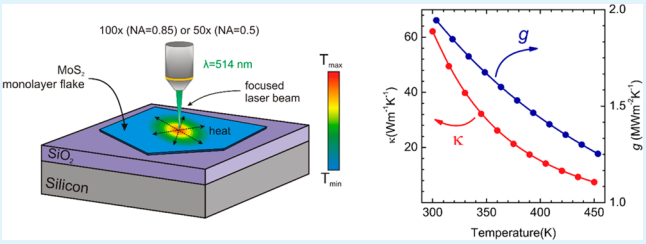

KEYWORDS: *molybdenum disulfide, MoS_2 monolayer, two-dimensional atomic crystals, Raman spectroscopy, thermal conductivity, thermal properties*

The family of transition metal dichalcogenides (TMDCs) consists of a number of compounds with the general formula MX_2, where M is a metal atom (e.g., W, Mo, Hf) and X is an atom of tellurium (Te), sulfur (S) or selenium (Se).[1] Isolated monolayers of transition metal dichalcogenides belong to a novel class of materials, two-dimensional atomic crystals,[2] which have gained much attention because of their unique electronic, optical and mechanical properties.[3−5] The most widely studied member of TMDC-based two-dimensional atomic crystals is molybdenum disulfide (MoS_2) monolayer, a semiconductor with a direct band gap of 1.85 eV.[6] Contrary to graphene, which is a semimetal with zero band gap, MoS_2 enables construction of a variety of electronic and optoelectronic devices, such as photodetectors,[7] transistors[8] and even integrated circuits.[9] For the operation and design of these devices, especially with constantly decreasing dimensions and increasing density of modern ultralarge-scale integrated circuits, knowledge of the thermal properties of the materials, such as thermal conductivity and interfacial thermal conductance, is essential. The thermal properties of MoS_2 are not yet fully understood, and there have been only a few theoretical[10,11] and experimental studies of molybdenum disulfide thermal conductivity.[12,13] However, in those reports, the temperature dependence of the thermal properties was not investigated and the studies were not strictly devoted to supported MoS_2 monolayers, i.e., the configuration most commonly used in real devices.[8]

The state-of-the-art method for nondestructive and reliable characterization of thermal properties of nanomaterials is currently an optothermal method based on Raman spectroscopy,[14−16] which is also used to determine the number of layers in two-dimensional atomic crystals.[17−19] For example, the thermal conductivity of graphene was measured for the first time using this method.[20] In this work, we report an experimental investigation of the thermal properties of MoS_2 single layers supported on SiO_2/Si substrates. Importantly, the temperature dependence of the thermal conductivity and interfacial thermal conductance values were determined, providing a valuable contribution to the understanding of the properties of two-dimensional atomic crystals. Our results may also be helpful in the design of MoS_2 electronic and optical devices.

The thermal conductivity (κ), interfacial thermal conductance per unit area (g), and temperature dependence were extracted from Raman spectroscopy measurements (scheme of experimental setup is shown in Figure 1a) using the approach developed by Cai et al.[15] In this model, the temperature distribution in the MoS_2 monolayer is obtained from the heat diffusion equation in cylindrical coordinates in the following form

$$\frac{1}{r}\frac{d}{dr}\left(r\frac{dT}{dr}\right) - \frac{g}{\kappa t}(T - T_a) + \frac{Q}{\kappa} = 0 \quad (1)$$

where g is the interfacial thermal conductance per unit area, κ is the thermal conductivity of supported MoS_2 monolayers, and t is the MoS_2 monolayer thickness. The volumetric optical heating, Q, is expressed by eq 2, assuming a Gaussian beam profile

$$Q = \frac{q_0}{t}e^{(-r^2/r_0^2)} \quad (2)$$

Received: January 23, 2015
Accepted: February 23, 2015
Published: February 23, 2015

DOI: 10.1021/acsami.5b00690
ACS Appl. Mater. Interfaces 2015, 7, 5061−5065

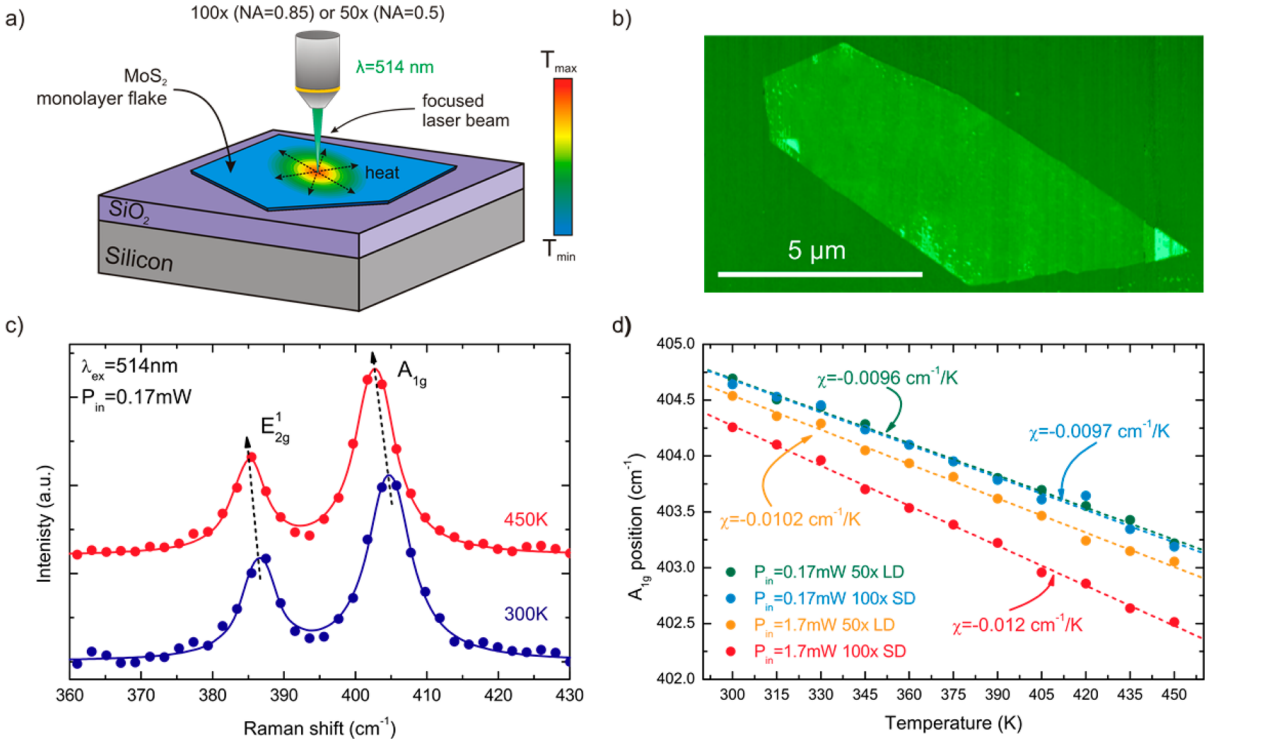

Figure 1. (a) Schematic of the experimental setup. (b) AFM image of a typical MoS_2 monolayer flake. (c) Raman spectrum of the MoS_2 monolayer at 300 and 450 K. (d) Temperature dependence of the MoS_2 monolayer A_{1g} mode for low incident laser power and upon laser heating for two different objectives—50× and 100×.

In the above equation, q_0 is the peak of absorbed laser power per unit area at the center of the beam spot.

We note that this model assumes diffusive phonon transport. For the MoS_2 monolayer, the phonon mean free path is on the order of a few to tens of nanometers,[10,11] much less than the utilized laser beam size, which validates the above assumption in our case.

The temperature rise due to optical power heating is defined as $\theta = T - T_a$, where T_a is the global temperature and T is the temperature in MoS_2 upon laser heating. Using the solution of eq 1, the temperature rise induced by laser beam irradiation measured by Raman spectroscopy method is expressed as follows[15]

$$\theta_m(\kappa, g, r_0) = \frac{\int_0^\infty \theta(r) e^{(-r^2/r_0^2)} r\,dr}{\int_0^\infty e^{(-r^2/r_0^2)} r\,dr} \quad (3)$$

However, instead of using eq 3 for calculating κ and g, the quantity $(\partial\theta_m/\partial P_{abs})$ (P_{abs} is total absorbed laser power) is used, which can be experimentally obtained using the following relation

$$\frac{\partial\theta_m}{\partial P_{abs}} = \frac{\partial\omega}{\partial P_{abs}}\frac{\partial\theta_m}{\partial\omega} = \frac{\partial\omega}{\partial P_{abs}}\chi^{-1} \quad (4)$$

The use of $(\partial\theta_m/\partial P_{abs})$ instead of θ_m for the determination of g and κ is to avoid artificial shifts of peak position resulting from calibration errors for two different objectives. The solution of eq 4 depends on 2 parameters: κ and g. The values of thermal conductivity and interfacial thermal conductance can be determined by solving a system of two eqs 4 for two $(\partial\theta_m/\partial P_{abs})$ obtained from the Raman measurements with two objectives with different numerical apertures values i.e., for two different r_0 values.

MoS_2 flakes were deposited by the conventional mechanical exfoliation method[2] on SiO_2 (275 nm)/Si substrates. Optical microscopy, atomic force microscopy (AFM) and Raman spectroscopy were used to locate and identify the monolayers. Figure 1b shows an AFM image of an exemplary, isolated single layer flake, whose thickness was approximately 0.7 nm, typical for a MoS_2 monolayer on a SiO_2 substrate.[8] Temperature-dependent Raman scattering studies were conducted using an Ar laser with a 514 nm (2.41 eV) excitation wavelength. The spectra were collected in the temperature range of 300 to 450 K using 50× (NA=0.5) and 100× (NA=0.85) objectives in ambient atmosphere. For each temperature and objective, measurements were performed at two incident laser radiation powers, 0.17 mW and 1.7 mW, which were calibrated on the sample. The Raman spectra of the MoS_2 monolayers and their corresponding Lorentzian fits taken at 300 and 450 K with low incident laser power (0.17 mW) are shown in Figure 1c. The Raman spectra of the MoS_2 monolayers taken with λ_{ex} = 514 nm shows two main modes, E^1_{2g} and A_{1g}. The E^1_{2g} mode is associated with in-plane vibration of the sulfur and molybdenum atoms, whereas the A_{1g} mode is related to out-of-plane vibration of sulfur atoms. At 300 K, the positions of the E^1_{2g} and A_{1g} modes were 386.4 cm^{-1} and 404.6 cm^{-1}, respectively. The difference between the positions of the two main Raman modes, which is typically used for determination of the number of MoS_2 layers, was 18.2 cm cm^{-1}, i.e., the value of monolayer MoS_2.[17] The position of the Raman peaks of MoS_2 monolayers is red-shifted with increasing temperature, as seen in Figure 1c, and thus it can be used as a temperature indicator. For the spectra measured at 450 K, the positions of E^1_{2g} and A_{1g} were 385.4 and 403.2 cm^{-1}, respectively, as

DOI: 10.1021/acsami.5b00690
ACS Appl. Mater. Interfaces 2015, 7, 5061−5065

determined from the Lorentzian fit. The full temperature dependence of the A_{1g} mode position measured between 300 and 450 K is depicted in Figure 1d. The position of the A_{1g} mode decreases with increasing global temperature for all cases and exhibits linear temperature dependence in the range used in the experiment. The experimental data were fitted to the following equation

$$\omega(T) = \omega_0 + \chi T \tag{5}$$

which is widely used to describe the temperature dependence of Raman modes in a wide group of materials, including MoS_2 and other two-dimensional crystals.[21−23] The extracted χ values were −0.0096 and −0.0097 cm^{-1}/K for low P_{in}. The slopes of the temperature dependence of the A_{1g} mode obtained from the data for higher P_{in} were greater at approximately −0.01 and −0.012 cm^{-1}/K for 50× and 100× objectives, respectively.

The laser beam size, r_0, is experimentally obtained by measuring the intensity of the silicon peak at ∼520 cm^{-1} as a function of distance (x) from the edge of the evaporated Au metallization on the SiO_2/Si substrate using a procedure similar to the "knife edge" method.[24] Figure 2a shows the obtained normalized intensity of the silicon Raman peak measured for two objectives used in Raman spectroscopy measurements with 100× and 50× magnification. The beam size is determined by fitting the experimental data to an error function with the following form

$$I(x) = (I_0/2)\left(1 + \mathrm{erf}\left(\frac{x - x_c}{x_0}\right)\right) \tag{6}$$

where x_0 is the beam size (r_0). The determined beam sizes for 100× and 50× objectives were 0.4 and 0.72 μm, respectively. We also checked the position of the Si substrate mode during laser heating and found that absorption of laser power caused a negligible temperature rise in silicon in our case.

For each fixed global temperature (without laser heating), $(\partial\theta_m/\partial P_{abs})$ was calculated as follows. First, the $(\partial\omega/\partial P_{abs})$ was calculated as the difference of the A_{1g} mode position measured for two different total absorbed laser powers divided by the P_{abs} difference, followed by linear fitting of the data (Figure 2b). The total absorbed laser power for the MoS_2 monolayer used in eq 2 was calculated as P_{in} times the absorbance level at the applied incident photon energy. The absorbance (α) level at 2.41 eV (λ = 514 nm) experimentally determined for monolayer MoS_2 varies between 4% and 9%[25−27] but was taken as 7% in our calculation. Then, we extrapolated the fitted data, i.e., the position of the A_{1g} mode for P_{abs} = 0. On the basis of this method, the temperature dependence of A_{1g} was obtained, and the temperature dependence coefficient, $\chi = (\partial\omega/\partial T)$, for P_{abs} = 0 was extracted. Finally, $(\partial\theta_m/\partial P_{abs})$ and the temperature rise upon laser heating, $\Delta T_{Raman} = \theta_m - T_a$, were calculated on the basis of eq 4.

The temperature dependence of $(\partial\theta_m/\partial P_{abs})$ and ΔT_{Raman} is presented in Figure 2c, d. First of all, both the measured thermal resistance and the temperature rise induced by laser heating were greater at 100× objective than at 50×. In both cases, $(\partial\theta_m/\partial P_{abs})$ and ΔT_{Raman} increased linearly with increasing global temperature. Note that the temperature rise determined by Raman spectroscopy at 100x increases more rapidly with global temperature than at 50×. For example, ΔT_{Raman} extracted at 300 K and an incident laser power of 1.7 mW for the 100× objective was 49.3 K, whereas it was 17.6 K for the 50x objective. At 450 K, ΔT_{Raman} was determined to be

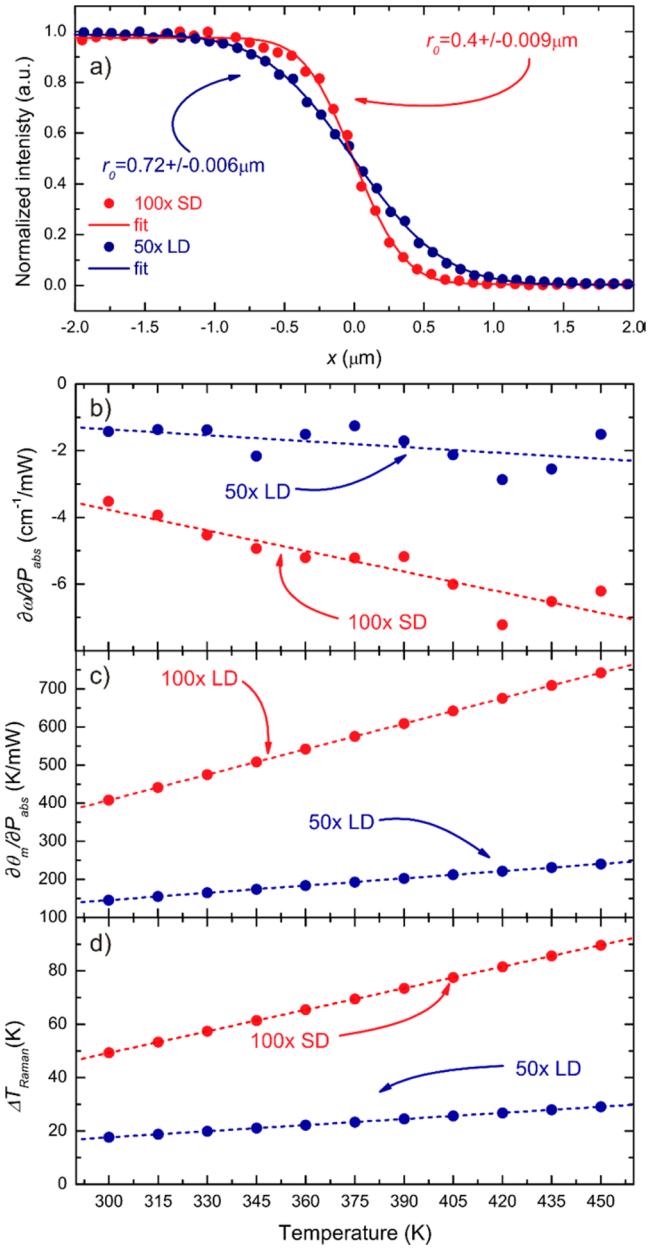

Figure 2. (a) Normalized Raman intensity of the Si peak as a function of beam position across the sharp edge of the Au film on the SiO_2/Si substrate used for determination of the laser beam size for 100× (red) and 50× (blue) objectives. Experimental data are shown as dots, where the lines represent the fit to eq 6. (b) Calculated dependence of the A_{1g} position on absorbed laser power for different global temperatures determined from Raman measurements. (c) $(\partial\theta_m/\partial P_{abs})$ values for different global temperatures determined from Raman measurements. (d) Temperature rise of MoS_2 monolayer upon laser heating for different global temperatures.

89.6 and 29.1 K for 100× and 50× objectives, respectively. These results can be explained by the different power densities focused on the surface of the monolayer flake (see Figures S1 and S2 in the Supporting Information).

The calculated thermal conductivity and interfacial thermal conductance values of MoS_2 supported on a SiO_2/Si substrate for different global temperatures are depicted in Figure 3. Similar to graphene, the thermal conductivity of the MoS_2 monolayer decreased with increasing temperature.[14] The trend of decreased thermal conductivity with increasing temperature

DOI: 10.1021/acsami.5b00690
ACS Appl. Mater. Interfaces 2015, 7, 5061−5065

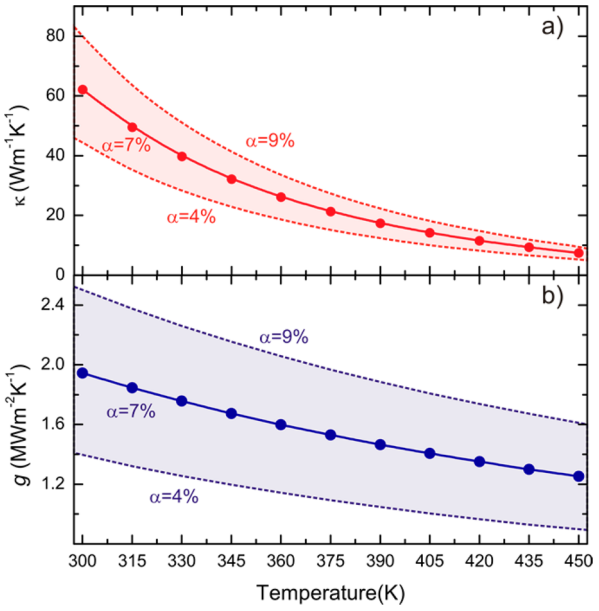

Figure 3. Calculated temperature dependence of (a) the thermal conductivity and (b) interfacial thermal conductance per unit area of supported MoS_2 monolayers. The shaded areas correspond to the minimum and the maximum of the absorbance values of MoS_2 monolayers reported so far.[25−27]

is related to the increased anharmonic scattering of phonons that contributed to the measured κ,[15] which has been observed in the temperature-dependent Raman study (Figure 1d). At 300 K, κ and g of the supported MoS_2 monolayer were calculated as 62.2 W m^{-1} K^{-1} and 1.94 MW m^{-2} K^{-1}, respectively. The shaded areas correspond to the minimum and the maximum of the absorbance values for MoS_2 monolayer reported so far. For instance, the change of the α by 2% causes almost 28% change in the value of κ and g. The value of the thermal conductivity of the supported MoS_2 monolayer was slightly higher than the previously determined value of a suspended MoS_2 monolayer[12] (34 W m^{-1} K^{-1}) and a multilayer[13] (52 W m^{-1} K^{-1}). This difference may be associated with the different sample preparation and measurement procedures. We note for instance that previous measurements of the thermal conductivity of suspended MoS_2 were performed under vacuum, in contrast to our measurements, which were conducted in ambient air. This difference may substantially influence the measurement conditions and affect the obtained results. Moreover, our approach exhibits more applicable character; i.e., the measurements were performed under operating conditions similar to those for a variety of MoS_2-based devices.

We note that the value of the interfacial thermal conductance at the interface between MoS_2 monolayer and the substrate my substantially influence the value of κ. Our calculations showed that a 10% change of g will change κ by almost 50%.

Furthermore, it was reported that the thermal conductivity of graphene increases with decreasing number of graphene layers from approximately 1200 W m^{-1} K^{-1} for 8 layers to approximately 4000 W m^{-1} K^{-1} for the monolayer.[28] If a similar trend can be assumed for MoS_2, our results agree with the measurements of multilayer MoS_2 obtained by Sahoo et al.,[13] which take into account the decrease of κ associated with the interaction of monolayer MoS_2 with the substrate. Nonetheless, as we mention in the introduction, there have been only a few reports regarding the thermal conductivity of MoS_2 and other transition metal dichalcogenides mono and multilayers; thus, further work is still required to fully understand their thermal properties.

■ ASSOCIATED CONTENT

Supporting Information

Supporting calculations of temperature distribution profiles under laser heating. This material is available free of charge via the Internet at http://pubs.acs.org.

■ AUTHOR INFORMATION

Corresponding Author

*E-mail: zdrojek@if.pw.edu.pl.

Present Address

†Andrzej Taube is also with Institute of Electron Technology, Warsaw, Poland and with Institute of Microelectronics and Optoelectronics, Warsaw University of Technology, Warsaw, Poland.

Notes

The authors declare no competing financial interest.

■ ACKNOWLEDGMENTS

This work was supported by the Polish Ministry of Science and Higher Education within the Diamond Grant programme (0025/DIA/2013/42).

■ REFERENCES

(1) Chhowalla, M.; Shin, H. S.; Eda, G.; Li, L.-J.; Loh, K. P.; Zhang, H. The Chemistry of Two-Dimensional Layered Transition Metal Dichalcogenide Nanosheets. *Nat. Chem.* **2013**, *5*, 263−275.

(2) Novoselov, K. S.; Geim, A.; Morozov, S. V.; Jiang, D.; Katsnelson, M. I.; Grigorieva, I. V.; Dubonos, S. V.; Frisov, A. A. Two-dimensional Atomic Crystals. *Proc. Natl. Acad. Sci. U.S.A.* **2005**, *102*, 10451−10453.

(3) Wang, Q. H.; Kalantar-Zadeh, K.; Kis, A.; Coleman, J. N.; Strano, M. S. Electronics and Optoelectronics of Two-Dimensional Transition Metal Dichalcogenides. *Nat. Nanotechnol.* **2012**, *7*, 699−712.

(4) Gaur, A. P. S.; Sahoo, S.; Ahmadi, M.; Dash, S. P.; Guinel, M. J.-F.; Katiyar, R. S. Surface Energy Engineering for Tunable Wettability through Controlled Synthesis of MoS_2. *Nano Lett.* **2014**, *14*, 4314−4321.

(5) Gaur, A. P. S.; Sahoo, S.; Ahmadi, M.; Guinel, M. J.-F.; Gupta, S. K.; Pandey, R.; Dey, S. K.; Katiyar, R. S. Optical and Vibrational Studies of Partially Edge-Terminated Vertically Aligned Nanocrystalline MoS_2 Thin Films. *J. Phys. Chem. C* **2013**, *117*, 26262−26268.

(6) Splendiani, A.; Sun, L.; Zhang, Y.; Li, T.; Kim, J.; Chim, C.-Y.; Galli, G.; Wang, F. Emerging Photoluminescence in Monolayer MoS_2. *Nano Lett.* **2010**, *10*, 1271−1275.

(7) Lopez-Sanchez, O.; Lembke, D.; Kayci, M.; Radenovic, A.; Kis, A. Ultrasensitive Photodetectors Based on Monolayer MoS_2. *Nat. Nanotechnol.* **2013**, *8*, 497−501.

(8) Radisavljevic, B.; Radenovic, A.; Brivio, J.; Giacometti, V.; Kis, A. Single-Layer MoS_2 Transistors. *Nat. Nanotechnol.* **2011**, *6*, 147−150.

(9) Wang, H.; Yu, L.; Lee, Y.-H.; Shi, Y.; Hsu, A.; Chin, M. L.; Li, L.-J.; Dubey, M.; Kong, J.; Palacios, T. Integrated Circuits Based on Bilayer MoS_2 Transistors. *Nano Lett.* **2012**, *12*, 4674−4680.

(10) Liu, X.; Zhang, G.; Pei, Q.-X.; Zhang, Y.-W. Phonon Thermal Conductivity of Monolayer MoS_2 Sheet and Nanoribbons. *Appl. Phys. Lett.* **2013**, *103*, 133113.

(11) Cai, Y.; Lan, J.; Zhang, G.; Zhang, Y.-W. Lattice Vibrational Modes and Phonon Thermal Conductivity of Monolayer MoS_2. *Phys. Rev. B* **2014**, *89*, 035438.

(12) Yan, R.; Simpson, J. R.; Bertolazzi, S.; Brivio, J.; Watson, M.; Wu, X.; Kis, A.; Luo, T.; Hight Walker, A. R.; Xing, H. G. Thermal Conductivity of Monolayer Molybdenum Disulfide Obtained from

DOI: 10.1021/acsami.5b00690
ACS Appl. Mater. Interfaces 2015, 7, 5061−5065

Temperature-Dependent Raman Spectroscopy. *ACS Nano* **2014**, *8*, 986−993.
(13) Sahoo, S.; Gaur, A. P. S.; Ahmadi, M.; Guinel, M. J.-F.; Katiyar, R. S. Temperature-Dependent Raman Studies and Thermal Conductivity of Few-Layer MoS_2. *J. Phys. Chem. C* **2013**, *117*, 9042−9047.
(14) Balandin, A. A. Thermal Properties of Graphene and Nanostructured Carbon Materials. *Nat. Mater.* **2011**, *10*, 569−581.
(15) Cai, W.; Moore, A. L.; Zhu, Y.; Li, X.; Chen, S.; Shi, L.; Ruoff, R. S. Thermal Transport in Suspended and Supported Monolayer Graphene Grown by Chemical Vapor Deposition. *Nano Lett.* **2010**, *10*, 1645−1651.
(16) Sahoo, S.; Chitturi, V. R.; Agarwal, R.; Jiang, J.-W.; Katiyar, R. S. Thermal Conductivity of Freestanding Single Wall Carbon Nanotube Sheet by Raman Spectroscopy. *ACS Appl. Mater. Interfaces* **2014**, *6*, 19958−19965.
(17) Lee, C.; Yan, H.; Brus, L. E.; Heinz, T. F.; Hone, J.; Ryu, S. Anomalous Lattice Vibrations of Single-and Few-Layer MoS_2. *ACS Nano* **2010**, *4*, 2695−2700.
(18) Zeng, H.; Liu, G.-B.; Dai, J.; Yan, Y.; Zhu, B.; He, R.; Xie, L.; Xu, S.; Chen, X.; Yao, W.; Cui, X. Optical Signature of Symmetry Variations and Spin-Valley Coupling in Atomically Thin Tungsten Dichalcogenides. *Sci. Rep.* **2013**, *3*.
(19) Late, D. J.; Liu, B.; Matte, H. S. S. R.; Rao, C. N. R.; Dravid, V. P. Rapid Characterization of Ultrathin Layers of Chalcogenides on SiO_2/Si Substrates. *Adv. Funct. Mater.* **2012**, *22*, 1894−1905.
(20) Balandin, A. A.; Ghosh, S.; Bao, W.; Calizo, I.; Teweldebrhan, D.; Miao, F.; Lau, C. N. Superior Thermal Conductivity of Single-Layer Graphene. *Nano Lett.* **2008**, *8*, 902−907.
(21) Zhang, S.; Yang, J.; Xu, R.; Wang, F.; Li, W.; Ghufran, M.; Zhang, Y.-W.; Yu, Z.; Zhang, G.; Qin, Q.; Lu, Y. Extraordinary Photoluminescence and Strong Temperature/Angle-Dependent Raman Responses in Few-Layer Phosphorene. *ACS Nano* **2014**, *8*, 9590−9596.
(22) Lanzillo, N. A.; Birdwell, A. G.; Amani, M.; Crowne, F. J.; Shah, P. B.; Najmaei, S.; Liu, Z.; Ajayan, P. M.; Lou, J.; Dubey, M.; Nayak, S. K.; O'Regan, T. P. Temperature-Dependent Phonon Shifts in Monolayer MoS_2. *Appl. Phys. Lett.* **2013**, *103*, 093102.
(23) Taube, A.; Judek, J.; Jastrzębski, C.; Duzynska, A.; Świtkowski, K.; Zdrojek, M. Temperature-Dependent Nonlinear Phonon Shifts in a Supported MoS_2 Monolayer. *ACS Appl. Mater. Interfaces* **2014**, *6*, 8959−8963.
(24) De Araújo, M. A.; Silva, R.; de Lima, E.; Pereira, D. P.; de Oliveira, P. C. Measurement of Gaussian Laser Beam Radius Using the Knife-Edge Technique: Improvement on Data Analysis. *Appl. Opt.* **2009**, *48*, 393−396.
(25) Mak, K. F.; Lee, C.; Hone, J.; Shan, J.; Heinz, T. F. Atomically Thin MoS_2: A New Direct-Gap Semiconductor. *Phys. Rev. Lett.* **2010**, *105*, 136805.
(26) Bernardi, M.; Palummo, M.; Grossman, J. C. Extraordinary Sunlight Absorption and One Nanometer Thick Photovoltaics Using Two-Dimensional Monolayer Materials. *Nano Lett.* **2013**, *13*, 3664−3670.
(27) Lee, G.-H.; Yu, Y.-J.; Cui, X.; Petrone, N.; Lee, C.-H.; Choi, M. S.; Lee, D.-Y.; Lee, C.; Yoo, W. J.; Watanabe, K.; Taniguchi, T.; Nuckolls, C.; Kim, P.; Hone, J. Flexible and Transparent MoS_2 Field-Effect Transistors on Hexagonal Boron Nitride-Graphene Heterostructures. *ACS Nano* **2013**, *7*, 7931−7936.
(28) Ghosh, S.; Bao, W.; Nika, D. L.; Subrina, S.; Pokatilov, E. P.; Lau, C. N.; Balandin, A. A. Dimensional Crossover of Thermal Transport in Few-Layer Graphene. *Nat. Mater.* **2010**, *9*, 555−558.

DOI: 10.1021/acsami.5b00690
ACS Appl. Mater. Interfaces 2015, 7, 5061−5065